Modelling and simulation of a signal injection self-sensored drive

Alen Poljugan, Mark Sumner, Chris Gerada
School of Electrical Engineering, University of Nottingham, Nottingham, UK, NG7 2RD
eexap5@nottingham.ac.uk, eezms@exmail.nottingham.ac.uk, eezcg@exmail.nottingham.ac.uk
Unska 3, 10040 Zagreb, Croatia, fax. 0038516129705, tel. 0038598694182, eexap5@nottingham.ac.uk

***Abstract*- This paper presents a new induction motor model specifically developed for simulating self-sensored variable speed drives which employ signal injection based sensorless control techniques. The model is to be used to investigate improved filtering algorithms and closed loop speed controllers. The model employs a simple state space equivalent circuit based model of the induction machine, which is enhanced to include rotor slotting and main flux saturation effects. The improvement is obtained by including a variation of machine inductances variation with the rotor position and the flux position. The new model is verified against experimental results.**

***Keywords*- Electrical machine, Induction motor, Adjustable speed drive, Self-sensing control, Simulation**

I. INTRODUCTION

In signal injection self-sensored drives, position and speed estimation is obtained by tracking the machine's response to high frequency (HF) voltages superimposed onto the normal fundamental voltage. A position dependent signal caused by the slotting of the rotor can be extracted from the HF current waveforms. However saturation effects in the machine and non-linear inverter effects such as dead time can add significant distortion to the estimated position signal [1,2,3] which can significantly impair the response of the drive.

To enhance estimation accuracy, different disturbance compensation methods can be used, such as harmonic and sideband filters [4], compensation tables [2-4], adaptive disturbance identifiers [4] etc. The main drawback of these techniques is their influence on the drive control performance, mainly observed as a reduction of the control loop bandwidth. In the commissioning process of self-sensored drives, the controller parameters need to be tuned, and this is usually achieved by trail and error. In this work the aim is to create a machine model which can be used to investigate the influence of the speed estimation algorithm (including filters etc) on the overall drive control performance with the ultimate objective being to achieve a high bandwidth speed controller.

It should be noted that the aim is not to create a physically accurate machine model. This can be achieved using finite element (FE) modelling packages, but their complexity when added to real time control algorithms means that they require very long simulation times [9]. The simplified equivalent circuit model is computationally fast but does not contain any physical detail of the machine. The Dynamic Mesh Reluctance Model (DMRM) provides a certain compromise by combining detailed machine analysis and relatively fast computational time [7,8]. It is however, still too slow to be used for HF injection systems.

[9,10,13,14] combine a FE analysis with a phase variable model. A machine inductance variation with rotor position is obtained from FE analysis and is then incorporated as look up tables. [9,10] report a fast computation time and accurate modelling of the machine saturation, rotor slotting effect and cogging torque. A space-vector state model of an induction machine including the rotor slotting effect is described in [15]. This model considers a variation of the stator and rotor leakage inductance due to rotor and stator slotting and develops a space-vector state formulation useful for application to observers. The rotor slotting harmonic (RSH) frequency is accurately modelled but there is an amplitude mismatch when compared to experiment, and saturation effects are not included. In the winding function approach (WFA) a machine model is derived by means of winding functions where no symmetry is assumed [11,12]. All machine inductances are calculated directly from the geometry and the winding layout of the machine. The WFA shows good modelling accuracy. Its computational time is faster than FEM (2 hours vs 12 hours [11]) however it is still comparatively slow when complex realtime control is required.

The induction machine model derived here is an extension of the simple equivalent circuit model, modified to include rotor slotting and main flux saturation effects. The improvement is obtained by including a variation of machine inductance with the rotor position and the flux position. The paper is structured such that section II introduces the equations of the machine model while section III describes the key points of the modelling and implementation. In the section IV the tuning of the model parameters is presented along with a comparison of the simulation with experimental results.

II. THE INDUCTION MACHINE MODEL

The machine model proposed in this paper is derived from a general phase model of the induction machine i.e. in the a-b-c frame of reference [16]. In the following sections, the motor phase voltages and currents will be referred to as winding variables. From the equivalent circuit a general form of the equations in the a-b-c frame can be written in matrix form as follows:

$$\begin{bmatrix} U_{abcs} \\ U_{abcr} \end{bmatrix} = \begin{bmatrix} R_s & 0 \\ 0 & R_r \end{bmatrix} \cdot \begin{bmatrix} i_{abcs} \\ i_{abcr} \end{bmatrix} + \frac{d}{dt} \begin{bmatrix} \Psi_{abcs} \\ \Psi_{abcr} \end{bmatrix} = \quad (1)$$
$$= \begin{bmatrix} R_s & 0 \\ 0 & R_r \end{bmatrix} \cdot \begin{bmatrix} i_{abcs} \\ i_{abcr} \end{bmatrix} + \frac{d}{dt} \left(\begin{bmatrix} L_s & L_{sr}^{'} \\ L_{sr}^{T} & L_r^{'} \end{bmatrix} \cdot \begin{bmatrix} i_{abcs} \\ i_{abcr} \end{bmatrix} \right)$$

where subscript *s* denotes stator and subscript *r* rotor variables.

The resistance matrices R_s and R_r as well as the inductance matrices L_s, L_r and L_{sr} in (1) can be written as follows:

$$R_s = \begin{bmatrix} R_{as} & 0 & 0 \\ 0 & R_{bs} & 0 \\ 0 & 0 & R_{cs} \end{bmatrix}, \; R_r = \begin{bmatrix} R_{ar} & 0 & 0 \\ 0 & R_{br} & 0 \\ 0 & 0 & R_{cr} \end{bmatrix},$$

$$L_s = \begin{bmatrix} L_{ls} + L_{ms} & L_{sab} & L_{sac} \\ L_{sba} & L_{ls} + L_{ms} & L_{sbc} \\ L_{sca} & L_{scb} & L_{ls} + L_{ms} \end{bmatrix} \quad (2)$$

$$L_r = \begin{bmatrix} L_{lr} + L_{mr} & L_{rab} & L_{rac} \\ L_{rba} & L_{lr} + L_{mr} & L_{rbc} \\ L_{rca} & L_{rcb} & L_{lr} + L_{mr} \end{bmatrix},$$

$$L_{sr}^{'} = L_{ms} \begin{bmatrix} \cos\theta_r & \cos\left(\theta_r + \frac{2}{3}\pi\right) & \cos\left(\theta_r - \frac{2}{3}\pi\right) \\ \cos\left(\theta_r - \frac{2}{3}\pi\right) & \cos\theta_r & \cos\left(\theta_r + \frac{2}{3}\pi\right) \\ \cos\left(\theta_r + \frac{2}{3}\pi\right) & \cos\left(\theta_r - \frac{2}{3}\pi\right) & \cos\theta_r \end{bmatrix}$$

where R_s and R_r represent the stator and rotor resistance respectively, L_{ls} and L_{lr} are the stator and rotor leakage inductance, L_{ms} and L_{mr} are the magnetizing inductances, L_{sab}, …, L_{scb} are the stator mutual inductances and L_{rab}, …, L_{rcb} are the rotor mutual inductances. The rotor electrical angle is denoted by Θ_r. The model is implemented in the Matlab/Simulink environment.

In this basic model the rotor slotting effect is not represented and therefore it cannot be used in the simulation of a signal injection drive. In the next section this model will be extended to incorporate rotor slotting and saturation effects.

III. Modelling of the Machine Nonlinear Effects

A. *Rotor slotting and saturation effects incorporated in the stator leakage inductance*

In an induction motor, a non-constant air gap permeance results from the presence of the stator and/or rotor slots, asymmetry in the stator and/or rotor, eccentricity of the rotor and/or stator and due to magnetic saturation. A general expression describing the total airgap permeance wave is quite complex and unnecessary for this work, as only speed-related terms are required. For this reason, it can be assumed that the airgap of the machine is bounded by a smooth stator and slotted rotor, and the variation of the airgap permeance is created by the rotor slot openings only. The rotor slots will produce airgap permeance waves with a spatial distribution dependent on the number used [5]. A typical permeance wave description will consist of a constant component (dc term) and a superimposed ripple (ac term). The fundamental component of the rotor slot permeance interacts with the magnetizing component of the airgap MMF and this modulation process generates two harmonic components in the airgap flux density. The RSHs are impressed on the stator currents as a consequence of the modulation of the machine's fundamental magnetic field and the airgap permeance wave produced by the rotor slots. The magnitude of these components varies little with applied load, except in machines with the closed rotor slots. The frequencies of these harmonics components will be given by [5,6]:

$$f_{RSH} = \upsilon \cdot \frac{N_R}{pp} \cdot f_r \pm k \cdot f_e \quad (3)$$

where f_{RSH} is the rotor slot harmonic frequency, υ is the RSH order, N_r is the total number of rotor slots, pp is the number of pole pairs, f_r is the mechanical frequency of the rotor rotation and f_e is the supply frequency. As can be seen from equation (3), the RSH frequencies are speed dependent and can be used to track the rotor speed [6]. In the following discussion these two components will be denoted as +1RSH and -1RSH, respectively.

To model the rotor slotting effects on the phase currents, only the stator leakage inductance in the equivalent induction motor model is considered to change in a periodic manner with rotor position. From the theoretical point of view, the rotor slotting effect will also affect other inductances in the machine [9,13,21,22] but here, for simplicity only the contribution of the stator leakage inductance was considered. The profile of the stator leakage inductance, presented in Fig. 1, is chosen following [9, 20] and also by using a DMRM simulation. The presented profile can be described with the following mathematical expression:

$$L_{lsa} = L_{ls\_DC} + k_{rs1} \sin[\frac{N_r}{pp} \cdot \Theta_r + \phi_1] + k_{rs2} \sin[(\frac{N_r}{pp} \Theta_r - pp \cdot \Theta_f) + \phi_2] \quad (4)$$

where L_{lsa} is the modified total stator leakage inductance of the phase a, L_{ls_DC} is the dc component of the leakage inductance, Θ_f is the stator flux position, k_{rs1},k_{rs2} and Φ_1 ,Φ_2 are the amplitudes and phase displacements of the ac inductance components.

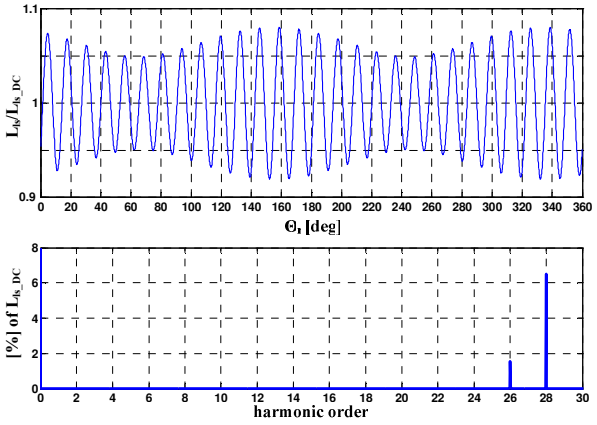

Fig. 1. Stator leakage inductance as a function of the rotor position. (top) and the frequency spectrum of the inductance profile (bottom)

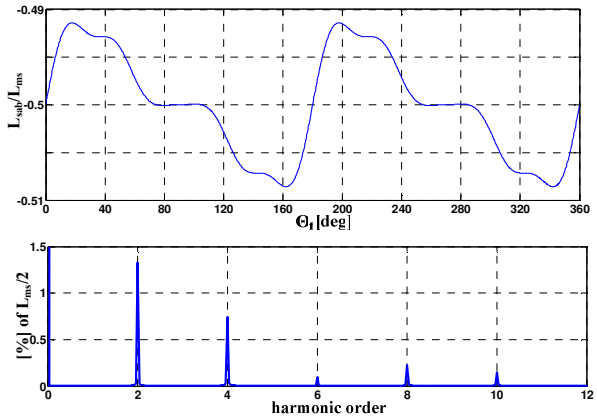

Fig. 2. Stator mutual inductance as a function of the stator flux angle (top) and the frequency spectrum of the inductance profile (bottom)

The new profile consists of a dc component superimposed with two ac components, as shown in Fig. 2. The component $28\Theta_r$ (N_r/pp=56/2) represents an airgap permeance wave caused by a slotted rotor, while the component $28\Theta_r$-$2\Theta_f$ represents a saturation sideband modulated by the RSH [20].

B. *Saturation effect incorporated in the stator mutual inductance*

Previous studies [17,18] show that saturation of the stator and rotor teeth is important as a much higher flux density exists in these locations. Since the flux density vector is rotating, the saturation regions will rotate too, modifying the tooth permeability in a cyclic manner resulting in a variation of the stator winding inductances. For simplicity, it will be assumed that only the stator mutual inductances will be modulated by the cyclic variation of tooth saturation. The authors in [17] propose a variation described with a simple mathematical equation. Although they present good results, there is only one tuning parameter available to adjust the magnitude of the saturation harmonics. For the simulation of a signal injection drive, a larger degree of fine tuning of the saturation harmonic components is desirable. Following analysis of the profiles obtained from FEM analysis

$$L_{sab} = L_{sba} = -\frac{Lms}{2}[1 + k_{s2}\sin(pp\cdot\Theta_f + \rho_1) + k_{s4}\sin(2\cdot pp\cdot\Theta_f + \rho_2) + \\ + k_{s6}\sin(3\cdot pp\cdot\Theta_f + \rho_3) + k_{s8}\sin(4\cdot pp\cdot\Theta_f + \rho_4) + \\ + k_{s10}\sin(5\cdot pp\cdot\Theta_f + \rho_5)] \quad (5$$

[9,13,20,21], the following expression was chosen to incorporate the saturation effects in the stator mutual inductance:

where k_{s2}, k_{s4}, k_{s6}, k_{s8} and k_{s10} are amplitudes and ρ_1,.., ρ_5 are phase displacements of the permeance wave introduced by tooth saturation. The mutual inductance profiles L_{sac}=L_{sca} and L_{sbc}=L_{scb} are a similar shape. For a four-pole machine the inductance profile consists of components at 2, 4, 6, 8 and 10 Θ_f as shown in Fig. 2. The parameters of the stator leakage and mutual inductance profiles are adjusted according to experimental measurements, as presented in the next section.

IV. SIMULATION RESULTS AND EXPERIMENTAL VERIFICATION

A four-pole, 30kW delta connected machine with 56 rotor slots is modelled. The machine has non-skewed semi-closed slots, and is part of an experimental system. The basic model is extended with the stator leakage and mutual inductance variation described in section III. The inductance variations are incorporated using (4) and (5). The simulation and experimental system also incorporated an indirect rotor field orientated control (IRFO) as well as the $\alpha\beta$ signal injection position estimation scheme described in [2-4].

A. *Model parameter tuning*

The parameters of the rotor slotting and saturation model are adjusted as follows. First the parameters of the rotor slotting model were tuned. The model is first simulated without the signal injection algorithm. The parameter k_{rs1} of the rotor slotting model is adjusted in such a way as to match the level of the +1RSH in the simulation to the one measured from the experimental line current. The -1RSH is present only in the phase current.

When operation with signal injection is considered, experimental investigation showed that the response of the machine model to the HF voltage does not match the experimental measurements. For the same injection voltage signal (778Hz and 37V_{peak}), it can be noticed that the current response at the HF frequency is approximately four times smaller than the experiment (1.4A compared to 5.9A). Nevertheless the relative amplitude of the RSH component modulated by injected signal is the same (approximately 3.3%). The relative amplitude is defined as the percentage of the excitation current component at the injection frequency. Although the problem with the small absolute magnitude may lead to signal processing issues, the initial results using the position estimation algorithm indicated that the absolute amplitude mismatch was not important when considering the ultimate application of the model.

Once the amplitude of the slotting harmonic has been adjusted, the saturation model can be tuned to match fundamental frequency related saturation components (i.e. 5^{th}, 7^{th}, etc.). However, when this method is used, the relative amplitude of the saturation components around the injection frequency will not match those observed in the experimental system. This again is due to the fact that the number of parameters adjusted in the model is kept low for simplicity, and therefore the model does not necessarily represent the true behaviour of the real machine. Non-linear frequency dependent variations neglected here include skin effect and eddy currents – to add these would over-complicate the model for the purpose intended. Therefore as this model is used specifically for investigation of signal injection techniques, the saturation model should be tuned for the response at the injection frequency.

In the position estimation process the measured line current is processed using a demodulation scheme described in [2-4] which ultimately gives the current position signals $i_{p\alpha}$ and $i_{p\beta}$, as shown Fig. 3. From the current position signals the rotor slot position is obtained using an *arctan* function or a phase locked loop. In the ideal case the current position signal spectrum will consist only of the rotor slotting component $28f_r$. However, saturation components modulated by the injected signal will appear in the current position signal and they represent a significant disturbance to the estimation process [2]. As the main aim of this research is to investigate disturbance elimination techniques and their influence on the drive control performance, the region around the injection

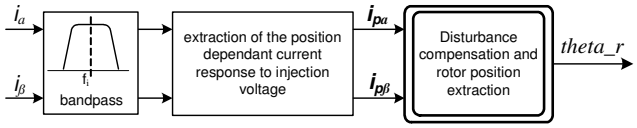

Fig. 3. Position estimation scheme in the signal injection drive

signal frequency is very important and the saturation model is adjusted according to the spectrum of the current position signal. By adjusting parameters k_{s2}, k_{s4}, k_{s6}, k_{s8} k_{s10} and k_{rs2} all the saturation harmonic components in the current position signal can be matched to experimental measurement. An adjustment of the saturation harmonic component in the current position signal will also cause a change in the harmonic spectrum around fundamental slotting harmonic +1RSH.

B. Operation around Fundamental Frequency

In the Fig. 4. and Fig. 5. results at 150 rpm and no load are presented. From the results it can be seen that parameters of the model have been adjusted such that the magnitude of the simulated +1RSH component matches the experimental results, also shown in Table I. There is slight mismatch in the amplitude of the +/-1RSH saturation sidebands because the saturation model has been tuned to match the harmonic content around the injection frequency, mentioned earlier. The biggest mismatch is in the magnitude of the 5th and 7th harmonic components. With regard to the machine model application tooth saturation is the most important saturation phenomena and core saturation in this case is neglected. By introducing a core saturation component to the model this mismatch can be reduced, at the expense of a more complicated model [17,19].

In Fig. 6. and Fig. 7. results at 150 rpm and 30% of the nominal load are presented. From the experimental results it can be seen that loading will cause a relative amplitude decrease in all of the harmonic components considered, as shown in Table II. Although the absolute amplitude of each harmonic is increasing, their amplitude relative to the fundamental current component is decreasing. In the simulation, the magnitudes of the +1RSH component and +1RHS saturation sidebands show a tendency to decrease with load, but by a smaller amount compared to experiment. This probably results from the simplifications made in the modelling of the rotor slotting and saturation effect. The simulated fundamental saturation components (the 5th and 7th) show a tendency to increase with load whereas the opposite occurs in the experimental system as seen in Table II. Once again this can be attributed to the fact that core saturation has not been modelled.

C. Operation at signal injection frequency

The simulation model was also investigated for operation with HF voltage injection. In the drive a small magnitude ($37V_{peak}$) voltage signal was injected in the $\alpha\beta$ frame at the frequency of 778 Hz. The frequency spectrum of the simulated current position signal was compared with the experimental results, noting that the harmonic magnitude is expressed as a percentage of the current component at the injection frequency.

In Fig. 8. and Fig. 9. results at 150 rpm and no load are presented. The RSH component at the $28f_r$ and three main saturation components $2f_e$, $4f_e$ and $8f_e$ match those obtained from the experiment (Table III). For the components at $10f_e$ and $28f_r$-$2f_e$ an amplitude mismatch can be noticed. By adjusting the parameters (k_{s10} and k_{rs2}) the amplitudes of these harmonics can be matched to experimental results but this will then create some additional harmonic components around the fundamental slotting harmonic +1RSH, namely the -1RSH-$10f_e$, +1RSH-$10f_e$ and most importantly the +/-1RSH-$2f_e$ components. As can be noticed from Table I this component is already larger than that seen in the experimental system. If for example the parameter k_{rs2} is tuned to match the $28f_r$-$2f_e$ component, the -1RSH-$2f_e$ component will increase by up to 2% (more then half of the +1RSH), as seen in Fig. 5. A similar effect is present when the $10f_e$ component is tuned. Further investigation will hopefully prove that operation of the current controllers is not significantly affected by this phenomenon, and the parameters can then be tuned to match the $10f_e$ and $28f_r$-$2f_e$ components. In Fig. 10. and Fig. 11. results at 150 rpm and 30% load are presented. From the experimental results, the saturation components $2f_e$, $4f_e$ and $8f_e$ decrease significantly with load (Table IV). In the simulation results this decrease can also be seen but it is very small. It is obvious that in the high frequency region and under the load condition the saturation model is not modelling accurately the saturation phenomenon. But from the FEM analysis of [13,14,20,21] it is clear that the magnitude of the inductance component as well as its phase displacement will vary with the load. Further investigation of the inductance variation profile can be used for additional fine tuning, either through a FE simulation or experimental testing, if required. Also it can be seen that under load two new saturation components appear at 14 and $16f_e$, as shown in Fig. 9. In the simulation the magnitudes of these components are negligible. A modified saturation model was investigated which included the new harmonic components in the mutual inductance profile. The results showed that the 14 and $16f_e$ component can be modelled but again the tuning of these components caused additional components around fundamental RSH. As mentioned before, this only merits further investigation if a more detailed model is required.

Experimental results shown in Fig. 7 and 9, also include harmonic components at the 37, 60 and 67 Hz. The frequency of these components is not dependent on the supply frequency but the magnitudes do increase with load. The authors suspect that these components originate from asymmetry in the experimental system. The results from normal operation also showed small even harmonic components in the line current which also suggests an asymmetry problem, Fig.3 and 5.

As mentioned before, the main aim of this project was to find an induction machine model which gave a good compromise between the simulation time and modelling accuracy. The simulation model presented here is fast – 75s computation time for a 10s simulation of a DOL machine. For a 1s DMRM simulation (previously reported to be "fast"), a computation time of 946s is needed.

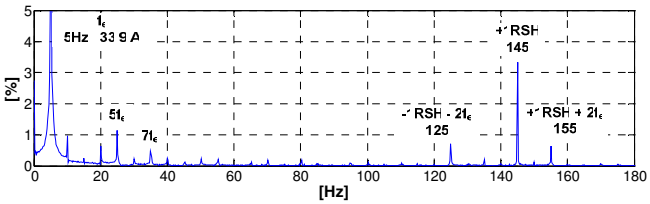

Fig. 4. Experimental results - frequency spectrum of the line current at 150 rpm and no load

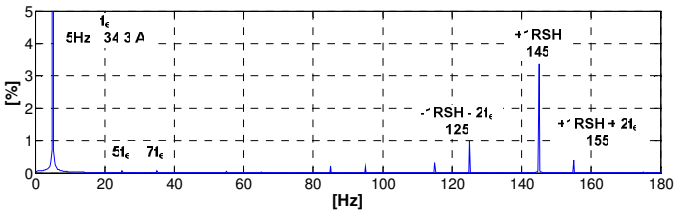

Fig. 5. Simulation results - frequency spectrum of the line current at 150 rpm and no load

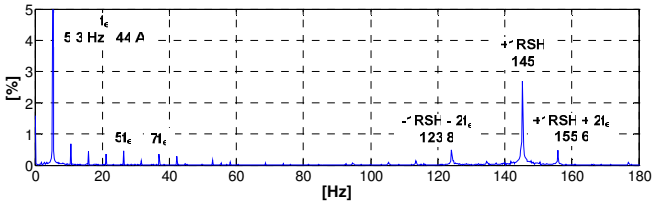

Fig. 6. Experimental results - frequency spectrum of the line current at 150 rpm and 30% of nominal load

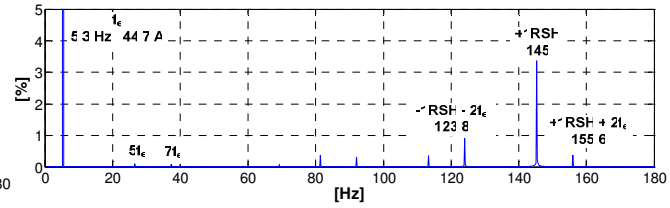

Fig. 7. Simulation results - frequency spectrum of the line current at 150 rpm and 30% of nominal load

TABLE I
HARMONIC SPECTRUM OF THE LINE CURRENT FOR NO LOAD CASE (%)

	5th	7th	+1RSH	-1RSH-2fe	+1RSH+2fe
experiment	1.13	0.48	3.35	0.72	0.63
simulation	0.06	0.07	3.37	0.98	0.39

TABLE II
HARMONIC SPECTRUM OF THE LINE CURRENT FOR 30% LOAD (%)

	5th	7th	+1RSH	-1RSH-2fe	+1RSH+2fe
experiment	0.45	0.35	2.69	0.5	0.48
simulation	0.08	0.09	3.31	0.9	0.38

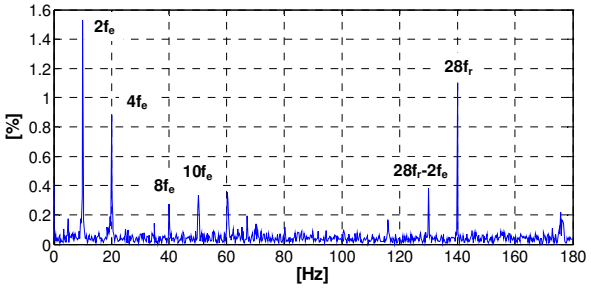

Fig. 8. Experimental results - frequency spectrum of the current position signal at 150 rpm, no load and hf injection

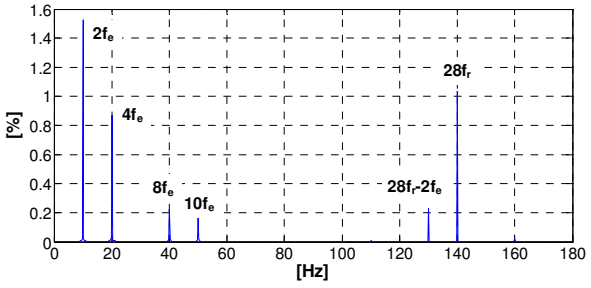

Fig. 9. Simulation results - frequency spectrum of the current position signal at 150 rpm, no load and hf injection

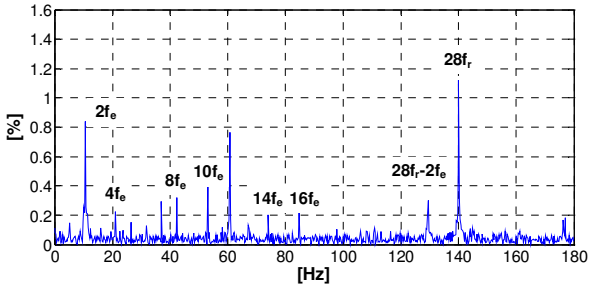

Fig. 10. Experimental results - frequency spectrum of the current position signal at 150 rpm, 30% of nominal load and hf injection

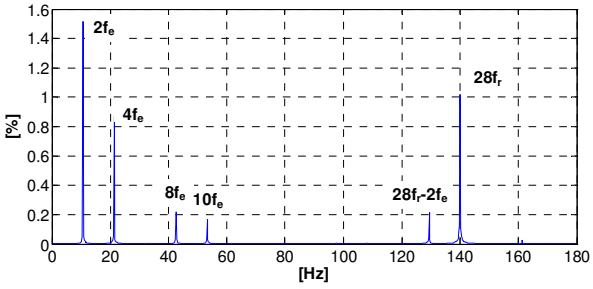

Fig. 11. Simulation results - frequency spectrum of the current position signal at 150 rpm, 30% of nominal load and hf injection

TABLE III
HARMONIC SPECTRUM OF THE LINE CURRENT FOR NO LOAD CASE AND HF INJECTION (%)

	$2f_e$	$4f_e$	$8f_e$	$10f_e$	$28f_r$ -$2f_e$	$28f_r$
experiment	1.53	0.88	0.28	0.33	0.38	1.1
simulation	1.53	0.87	0.22	0.17	0.23	1.04

TABLE IV
HARMONIC SPECTRUM OF THE LINE CURRENT FOR NO LOAD CASE AND HF INJECTION (%)

	$2f_e$	$4f_e$	$8f_e$	$10f_e$	$28f_r$ -$2f_e$	$28f_r$
experiment	0.84	0.22	0.32	0.42	0.3	1.12
simulation	1.51	0.86	0.21	0.16	0.21	1.02

V. CONCLUSION

This paper has presented a new induction motor model for use with developing signal injection based self-sensing induction motor control systems. A simple equivalent circuit model is improved with the rotor slotting and saturation effect.

The rotor slotting effect is incorporated as a rotor position dependant stator leakage inductance variation. The magnitudes of the rotor slotting harmonics can be adjusted to match those measured experimentally by means of tuning two parameters.

The saturation effect is incorporated as a flux position dependant component in the stator mutual inductance. The inductance profile consists of five harmonic components and the magnitude and phase displacement of each component can be adjusted. Considering the machine model application, the saturation model was tuned to match the experimental results around the injection frequency.

The results comparison shows that a relative magnitude of the rotor slotting harmonics match those obtained from the experiment for all loading conditions. The saturation model for the no load condition gives good results with a slight magnitude mismatch of two harmonic components ($10f_e$ and $28f_r$-$2f_e$). These components can be additionally tuned to match the experiment but this result in detuning of some harmonic components around the fundamental RSH. A further investigation will show how these components affect the current controller.

The proposed profiles of the machine inductances are not considered to be load dependant. Therefore under load conditions the saturation model shows poor results. If a more detailed model is required, variation of the inductance profiles with a load can be included (at extra computational cost).

ACKNOWLEDGMENT

The authors would like to acknowledge the support provided by the European Commission under a Marie Curie Research Training Network for realizing this work under the MEST-CT-2004-504243 Research Project.

REFERENCES

[1] J.I. Ha, S.K. Sul, "Sensorless Field-Orientation Control of an Induction Machine by High-Frequency Signal Injection", *IEEE Transactions on Industry Applications, Vol. 35, No. 1, Jan/Feb 1999*

[2] N. Teske, G. M. Asher, M. Sumner, and K. J. Bradley, "Suppression of Saturation Saliency Effects for the Sensorless Position Control of Induction Motor Drives under Loaded Conditions," *IEEE Transactions on Industrial Electronics, vol. 47, no. 5, pp. 1142 – 1150, Oct. 2000.*

[3] N. Teske, G.M. Asher, K.J. Bradley and M. Sumner, "Analysis and Suppression of Inverter Clamping Saliency in Sensorless Position Controlled Induction Machine Drives", *IEEE-IAS 2001, Proc. On CD ROM*

[4] Q. Gao, G. Asher and M. Sumner, "Sensorless Position and Speed Control of Induction Motors Using High Frequency Injection And Without off-line Pre Commissioning*", the 31st Annual Meeting of IEEE, IES 2005*

[5] A. Ferrah, P. J. Hogben-Laing, K. J. Bradley, G. M.Asher, and M. S. Woolfson, "The Effect of Rotor Design on Sensorless Speed Estimation Using Rotor Slot Harmonics Identified by Adaptive Digital Filtering Using the Maximum Likelihood Approach," *in Conf. Rec. IEEE–IAS Annual Meeting, , no. 32, pp. 128 – 135, Oct. 1997.*

[6] A. Ferrah,, K. J. Bradley, P. J. Hogben-Laing, M. S. Woolfson, G. M. Asher, M. Sumner, J. Cilia, and J. Shuli "A Speed Identifier for Induction Motor Drives Using Real-Time Adaptive Digital Filtering", ," *IEEE Transactions on Industry Applications, Vol. 34, No. 1, Jan/Feb 1998*

[7] C Gerada, K J Bradley, M Sumner and P Sewell, "Evaluation of a Vector Controlled Induction Motor Drive using the Dynamic Magnetic Circuit Model", *IEEE Transactions on Industry Applications, Vol. 43, No. 3, May/June 2007*

[8] P Sewell, KJ Bradley, JC Clare, PW Wheeler, A Ferrah, R Magill, S Sunter, "Dynamic Reluctance Mesh Modelling of Induction Motors" , *Proc ICEM'98 Istanbul, pp 1324 - 1329, Sept 1998*

[9] O. A. Mohammed, S. Liu, and Z. Liu, "Phase variable model of PM synchronous machines for integrated motor drives*," IEE Proc. Sci., Meas., Technol., vol. 151, no. 6, pp. 423–429, Nov. 2004.*

[10] O. A Mohammed, Z Liu, and S. Liu, "A novel sensorless control strategy of double-fed induction motor and its examination with the physical modeling of machines," *IEEE Transactions on Magnetics, Vol. 41, No. 5, May 2005, pp.1852-1855.*

[11] S. Nandi, "Modeling of Induction Machines Including Stator and Rotor Slot Effects" *IEEE Transactions on Industry Applications, vol. 40, no.5, Sep/Oct.. 2004.*

[12] S. Nandi, "A Detailed Model of Induction Machines With Saturation Extendable for Fault Analysis" *IEEE Transactions on on Industry Applicationss, vol. 40, no.5, Sep/Oct.. 2004.*

[13] N.A. Demerdash, P. Baldassar, "A combined finite element - state modeling environment for induction motors in the abc frame: the no-load condition", *IEEE Transactions on Energy Conversion, Vol. 7, No. 4. Dec. 1992.*

[14] P. Baldassari, N.A. Demerdash, "A combined finite element - state modeling environment for induction motors in the abc frame: the blocked rotor and sinusoidally energized conditions", *IEEE Transactions on Energy Conversion, Vol. 7, No. 4. Dec 1992.*

[15] M. Cirrincione, M. Pucci, G. Cirrincione, A. Miraoui, "Space-Vector State Model of Induction Machines Including Rotor and Stator Slotting Effects", *Electric Machines & Drives Conference, 2007. IEMDC '07. IEEE International Volume 1,May 2007*

[16] S.E. Lyshevski, *Electromechanical Systems, Electric Machines and Applied Mechatronics.* CRC Press, Boca Raton, Florida, 1999.

[17] V. Donescu, A. Charette, Z. Yao, and V. Rajagopalan, "Modeling and simulation of saturated induction motors in phase quantities," *IEEE Trans. Energy Conversion, vol. 14, pp. 386–393, Sept. 1999.*

[18] J. C. Moreira and T. A. Lipo, "Modeling of saturated AC machines including air gap flux harmonic components," *IEEE Trans. Ind. Applicat., vol. 28, pp. 343–349, Mar./Apr. 1992.*

[19] J.O. Ojo, A. Consoli, T.A. Lipo, "An Improved Model of Saturated Induction Machines", *IEEE Transactions on Industry Applications, Vol. 26, No. 2, MarchIApril 1990*

[20] S. Williamson, C.I. McClay, "The effect of axial variations in saturation due to skew on induction motor equivalent-circuit parameters", Industry Applications, *IEEE Trans on , Volume: 35 Issue: 6 , Nov.-Dec. 1999*

[21] C. Gerada, K.J. Bradley, M. Sumner, G. Asher, J. Arellano-Padilla, "Permanent Magnet Synchronous machines for Saliency-based, Self-Sensored Motion Control", *IEEE IECON 2007 Proc. On CD-ROM*